CrossMark

ORIGINAL CONTRIBUTION

Synthesis of silica Janus nanoparticles by buoyancy effect-induced desymmetrization process and their placement at the PS/PMMA interface

Esmail Sharifzadeh[1] · Mehdi Salami-Kalajahi[1] · Mahdi Salami Hosseini[2] · Mir Karim Razavi Aghjeh[2]

Abstract This work presents a unique desymmetrization method to produce a high quantity of Janus nanoparticles (JNPs) using dual-phase oil (melted wax)/water system. The four-stage process includes fixing, primary modification, releasing, and secondary modification. Unlike other works, dispersed hydrophilic nanoparticles were forced to be placed at oil/water interface using an upward water stream formed by buoyancy effects due to the applied heat to the bottom of the container. This eliminated some significant deficiencies of common desymmetrization processes which apply oil (melted wax)/water Pickering emulsion systems, e.g., the coalescence of melted /solidified wax droplets and high cost. The best effect of heat-driven buoyancy flow was ensured using saturation theory. In order to induce asymmetrical surface properties to the applied nanoparticles, (3-aminopropyl)triethoxysilane and hexadecyltrimethoxysilane were used in primary and secondary modification stages, respectively. Produced JNPs were characterized using FTIR, thermogravimetric analysis (TGA), and energy-dispersive X-ray spectroscopy (EDX) tests in order to confirm the attachment of modifier molecules on the surface of the applied nanoparticles. Furthermore, TGA results were used to calculate three-phase contact angle (β) as an important parameter dictating the asymmetric properties of Janus nanoparticles. Also, a dichloromethane/water mixture was used to demonstrate the differences of Janus nanoparticles with similar uniformly modified nanoparticles. Furthermore, using polystyrene/poly(methyl methacrylate) blend, it was shown that produced Janus nanoparticles tend to be placed at the interface while their corresponding uniformly modified nanoparticles stay in polystyrene or poly(methyl methacrylate) phase.

Keywords Janus nanoparticles · Asymmetrical surface modification · Pickering emulsions · Oil/water system · Surface characterization

✉ Mehdi Salami-Kalajahi
m.salami@sut.ac.ir

1 Department of Polymer Engineering, Sahand University of Technology, P.O. Box-1996, Tabriz 51335, Iran

2 Institute of Polymeric Materials, Sahand University of Technology, P.O. Box-1996, Tabriz 51335, Iran

Introduction

Colloidal nanoparticles represent very interesting building blocks in creating complex materials with unique properties in different practical fields [1]. Recently, there have been significant advances in preparing such nanomaterials as monodispersed nano-objects, and it is now the matter of tailoring of their properties via surface modification [2, 3] which has led to nanoparticles with isotropic surficial chemistry [4]. On the other hand, regioselective surficial modification (anisotropic surficial modification) is proved to be a good way to enhance and control the shape and properties of such nanomaterials [5, 6]. So far, many methods have been introduced to obtain a new generation of particles called Janus nanoparticles (JNPs) presenting dissymmetrical surficial chemistries [7–9]. Among all unique proposed methods, it is always the quantitative and qualitative efficiencies which indicate the capability of a method of producing JNPs. Desymmetrization in high internal interface systems is one of the most practical strategies that applies the privileges of Pickering emulsion systems to provide JNPs [10]. This approach implies that a wax-in-water emulsion is stabilized with

Springer

colloidal particles (e.g., nanoparticles) and forms so-called Pickering emulsion [11]. A Pickering emulsion is a two-phase oil/water emulsion system in which the interface is stabilized by colloidal beads via purely physical interactions [12]. The formation of such system is strongly favored with increasing particles size that explains the reason of challenge to produce Pickering emulsion using very small nanoparticles (<50 nm) [13]. Perro et al. applied Pickering emulsion of wax in water to produce high quantities of JNPs [10]. The process is based on dispersing melted paraffin wax in water media containing silica particles using a stirrer. It is reported that silica particles were trapped on the surface of oil droplets after cooling to temperatures lower than the melting point of paraffin wax. Thereafter, modification of exposed surface of trapped silica particles resulted in producing Janus particles. In another work, Jiang et al. tried to control the penetration depth of silica particles into the surface of oil droplets [14] To this end, they used different amounts of a specific secondary surfactant to change the hydrophilicity of silica particles that directly affects the penetration depth. Giermanska et al. kinetically investigated the stabilization of oil-in-water emulsions comprising paraffin-melted droplets by adsorbing silica particles at the oil/water interface [15]. Applying Pickering emulsion systems, Hong et al. proposed a new and very practical method to produce Janus particles in large quantity [16]. They used (3-aminopropyl)triethoxysilane (APTES) to chemically modify the exposed surface of adsorbed and immobilized particles on the surface of solidified paraffin droplets (SPDs). It seems that using high internal interface systems proposes a unique and efficient procedure to produce Janus particles (as well as JNP). However, there are still some significant process deficiencies (e.g., high energy consumption, material waste) which limit the application of the mentioned methods in industries.

To overcome the above-mentioned limitations, in this study, we propose a new four-step method comprising fixing, primary modification, releasing, and secondary modification stages to produce JNPs. As demonstrated in Scheme 1, the fixing process was performed using a dual-phase water/oil system in which silica nanoparticles, dispersed in the water phase, were forced to be placed at oil/water interface. Then, solidified paraffin substrate covered with silica nanoparticles at the bottom side was exposed to a primary modification stage in which the exposed surface of fixed nanoparticles was chemically modified using APTES. Afterward, the nanoparticles were separated from the substrate in the releasing stage and then were exposed to a secondary modification stage using hexadecyltrimethoxysilane (HDTMS).

In general, the novelty of this work can be categorized into four parts: (I) elimination of limited and partial coalescences as two different but very effective parameters in producing JNPs. Limited (relaxed) coalescence occurs between melted paraffin droplets and helps them to freely relax their shape [15]. On the other hand, partial (unrelaxed) coalescence implies that the solidified paraffin particles irreversibly connect and form paraffin bridge [15]. These parameters drastically decrease the quantitative efficiency of common desymmetrization processes [10]; (II) simple fixing without intensive mixing; (III) utilizing saturation theory (ST) that indicated the optimum required content of dispersed particles in the system based on the strength of heat-driven buoyancy flow; (IV) fixing of the primary hydrophilic nanoparticles on an individual paraffin planner surface (in the fixing stage) instead of thousands of thousands micron-sized (or smaller) SPDs [10, 14]. Also, FE-SEM, FTIR, energy-dispersive X-ray spectroscopy (EDX), and thermogravimetric analysis (TGA) were used to characterize the produced JNPs and confirm surface modification after each stage.

Experimental section

Materials

Paraffin wax as the oil phase, with a very narrow range of melting temperature from 56 to 58 °C and density of 0.9 g/cm^3, was purchased from Dr. Mojallali Industrial Chemical Co. (laboratory grade). Ethanol (Merck, 99.9%), APTES (Aldrich, 99%), HDTMS (Aldrich, ≥85%), chloroform (Dr. Mojallali Industrial Chemical Co., >99%), and dichloromethane (Merck, 99.9%) were used as received. Particle-stabilized emulsions were obtained using two different hydrophilic silica nanoparticles (Aerosil fumed silica), kindly provided by Degussa. Their characteristics are reported in Table 1. Polystyrene (PS) (Grade 1160 GPPS) was purchased from Tabriz Petrochemical Corporation. And poly (methyl methacrylate) (Grade E920) was purchased from LG Corporation.

Fixing stage

All paraffin substrates were primarily provided in 33.6 L (0.4 m × 0.7 m × 0.12 m) rectangular cube container heated only from its bottom side. The content of paraffin wax was precisely indicated to ensure that the final solidified substrates could tolerate the process physical conditions (e.g., transporting from one stage to another). It was experimentally indicated that a paraffin substrate with a thickness of 0.5 cm is completely capable of providing the process necessities and stays unbroken to the end of primary modification stage. Accordingly, the weight of required paraffin ($W_{paraffin}$) can be calculated by Eq. (1):

$$W_{paraffin} = 0.5 \times A_c \times \rho_{paraffin} \tag{1}$$

where $\rho_{paraffin}$ is the density of paraffin wax and A_c indicates the top surface area of the container. The system was considered to be governed by the saturation theory (ST) in that the content of the nanoparticles stays at its theoretical saturation

Scheme 1 Schematic of applied process to produce JNPs
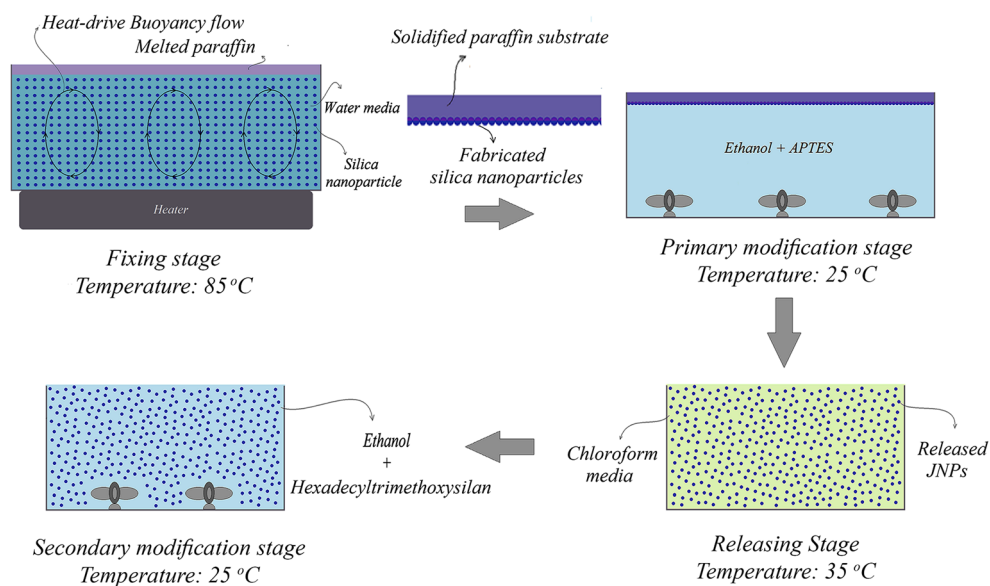
point in fixing stage. As illustrated in Scheme 2, the theory takes the applied water volume as an ensemble of similar small water cubes. It should be noted that the ratio of side lengths of the hypothetical cubes to the diameter of applied nanoparticles (R_{CD}) will be discussed later. Considering a spherical silica nanoparticle at the center of each hypothetical cube, the theory presents a unique strategy to calculate the saturating content of nanoparticles. In general, the theory takes six available directions for a spherical silica nanoparticle to strike its neighbors due to their thermal energy (Scheme 2d) [17]. As a result, if the content of silica nanoparticles stays at its saturation point, nanoparticles occupying the neighbor layer of oil/water interface (Scheme 2c) have a significant chance to be placed on the surface of paraffin substrate. Also, considering the upward water stream due to heat-driven buoyancy flow [18], it is suggested that nanoparticles at the vicinity of oil/water interface are driven to be placed at the interface due to thermodynamic factors of the system (Scheme 2c) [4, 19]. Accordingly, it is assumed that heat-driven buoyancy flow forces silica nanoparticles to fill all empty cubes placed in the neighbor layer of the oil/water interface (Scheme 2d). This definitely increases trapping chance of nanoparticles in the oil phase.

Heat-driven buoyancy flow was investigated via an hour tracing of dispersion of P2 nanoparticles in water media at 85 °C. The content of P2 nanoparticles in 500 mL of water was indicated by monitoring the effect of the flow on the dispersion of nanoparticles. Considering the water vaporization rate at 85 °C (experimentally indicated to be 1.2 mL min^{-1} at

85 °C), 72 mL of excess water was added to the system to monitor the results in exactly 500 mL of water during 1 h. Different amounts of P2 nanoparticles were added to the system in order to investigate the optimum effects of heat-driven buoyancy flow at the shortest possible test time. Considering $R_{CD} = 15$, complete dispersion of P2 nanoparticles was accomplished after 5 min and more importantly, there was no silica nanoparticle left at the bottom of the container that was ascribed to the proper functionality of heat-driven buoyancy flow. It should be noted that the further increase in the content of silica nanoparticles followed by their accumulation on the bottom of the container. Figure 1 shows the system, based on $R_{CD} = 15$, at the different process time points.

It was experimentally indicated that the minimal required temperature to form detectable heat-driven buoyancy in the system is about 40 °C, although this temperature should be set based on the melting point of the applied paraffin and best possible particle dispersion in the least possible time. On the other hand the maximal temperature should be below the boiling point of water.

Accordingly, theoretical saturating content of silica nanoparticles (W_{silica}) is given by Eq. (2) based on $R_{CD} = 15$:

$$W_{silica} = \frac{(V_c f - 0.5 A_c) \times (V_s\, \rho_{silica})}{(R_{CD}d)^3} \quad (2)$$

where ρ_{silica} is the density of nanoparticles ($\rho_{silica} = 2.2$ g cm^{-3}) [15], V_c is the total volume of the container, V_s is the volume

Table 1 Characteristics of utilized silica nanoparticles

Nanoparticle name	Commercial name	Nanoparticle diameter (nm)	Free silanol group density (nm^{-2})
P1	Aerosil A200	12	1.4
P2	Aerosil OX 50	40	1.9

Scheme 2 **a** The general structure of ST. **b** A water cube and its empty sub-cube constituents. **c** Side view of the general structure. **d** Possible striking directions for an individual silica nanoparticle
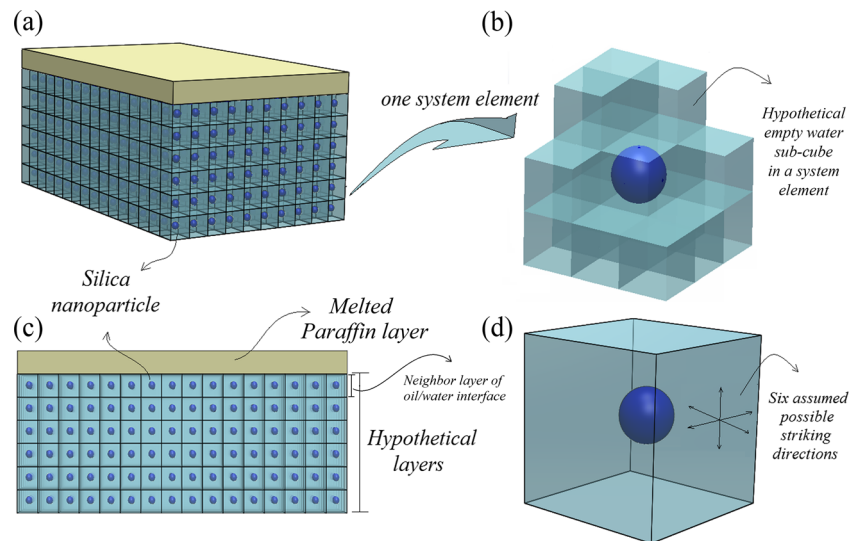
of a silica nanoparticle (considering a perfectly spherical shape $V_s = \pi d^3/6$), and f is the filling factor that was empirically indicated to be 0.95. Consequently, the volume of required water can be calculated using Eq. (3):

$$V_{water} = (f \times V_c - 0.5A_c) - \frac{W_{silica}}{\rho_{silica}} \qquad (3)$$

It should be noted that the content of silica nanoparticles should be essentially maintained at its theoretical saturation point (as stated by ST) during consecutive fixing processes. This will maximize the nanoparticle attachment probability to the oil/water interface. After adding 83 g of either silica nanoparticles to the water phase (Eq. (2)), the system was heated to 85 °C in order to melt down paraffin

wax as oil phase as well as inducing the effects of heat-driven buoyancy flow to the system. After 30 min, the system was cooled down to room temperature and the solidified paraffin substrate (covered by P1 or P2) was exposed several times to washing processes with deionized water in order to remove unattached and weakly attached nanoparticles. The schematic of fixing process on paraffin substrate is shown in Scheme 1.

In order to increase the amount of production, the entire process should be run continuously for several times. Therefore, after finishing fixing process for a paraffin substrate, the next substrate was replaced and the process was reinitiated after resetting the content of nanoparticles to reach its theoretical saturation point. The

Fig. 1 Effect of heat-driven buoyancy flow on dispersion of P2 nanoparticles ($R_{CD} = 15$) after **a** 0 s, **b** 75 s, **c** 90 s, **d** 2 min, **e** 5 min, **f** 25 min, **g** 50 min, and **h** 1 h
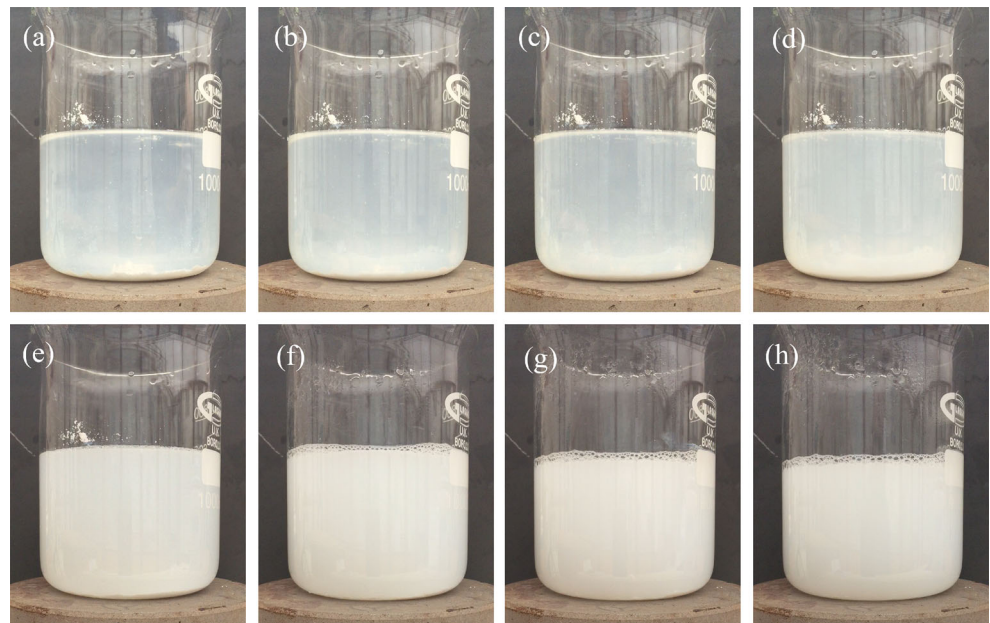
complementary required weight of nanoparticles (W_{CS}) after each fixing process can be calculated using Eq. (4):

$$W_{CS} = \left(\frac{A_c V_s \rho_{silica}}{d^2} \right) \quad (4)$$

It should be noted that Eq. (4) also indicates the amount process yield per each batch which is 3.87 (mg) for P1 JNPs and 12 (mg) for P2 JNP. Though, increasing A_C and/or number of bathes increase the process yield.

Utilizing the privileges of ST, it was possible to eliminate secondary surfactants which are commonly used in order to increase the tendency of silica nanoparticles (<50 nm) to be placed at oil/water interface [10, 16]. These materials significantly consume the preferential reactive sites on the surface of nanoparticles (e.g., –OH sites on the surface of hydrophilic silica nanoparticles) and decrease the efficiency of modification stage.

Add process yield, use *n* as number of batches. Introduce a parametric formula.

Primary modification stage

Paraffin substrates covered with P1 or P2 nanoparticles were immersed in a 0.2-vol% solution of APTES/ethanol at 25 °C (Fig. 1) [16]. The system was stirred at 500 rpm for 24 h. Then, the exposed surface of paraffin substrate was washed with ethanol to remove extra unattached APTES molecules.

Releasing stage

Considering the scale of the applied nanoparticles, a very thin layer of the substrate was shaved and then submerged in chloroform. This helped to prevent the entrance of excess paraffin into the solvent media since it is very important to eliminate the residual paraffin from final products. One milliliter of chloroform was used per 0.7 g of paraffin to accomplish the realizing process after 25 min at 35 °C. These values were indicated based on the chloroform saturation dependencies to the temperature and the paraffin concentration. Accordingly, indicating an optimized dissolving temperature as a function of paraffin content helped to increase the stage efficiency. We designed a simple method based on the procedure of indicating cloud point of ternary polymer systems [8, 20, 21]. The method was used to determine the cloud point of paraffin/chloroform solutions with different concentrations (0.1, 0.2, 0.3, 0.5, 0.7, and 0.9 g paraffin in 1 mL of chloroform) without agitating at 40 °C. After complete dissolution, the system was gradually cooled down (1–1.5 °C/min). At the first sight of turbidity, cooling process was stopped and the temperature was raised again to see whether or not the turbidity disappears at a specific cloud point. This procedure was repeated since the exact temperature was determined. The

process was traced using a high-resolution camera in order to increase the accuracy. At least 15 samples were tested for each composition to calculate average cloud points temperature (Fig. 2a). The amount of required chloroform per paraffin content (at a specific temperature) was also indicated in order to determine the proper amount of required solvent for the process (Fig. 2b).

Secondary modification stage

Released JNPs were dispersed in a mixture of 0.2 vol% HDTMS in ethanol. The system was stirred at 500 rpm for 24 h at 25 °C. The collected nanoparticles were washed with ethanol to remove unattached HDTMS molecules.

Characterization and instrumentation

FE-SEM (MIRA3, Tescan) device was used to investigate the presence of nanoparticles on the surface of provided paraffin substrates. The specimens were prepared by coating a thin layer on a mica surface using a spin coater (Modern Technology Development Institute, Iran). The cloud point test procedure was recorded using a high-resolution digital camera (HXR-MC1500, maximum optical magnification ×12, Sony). FTIR spectra were recorded on a Fourier transform infrared spectrometry (Tensor 27, Bruker) using KBr in the infrared region of 400–4000 cm^{-1}. TGA were conducted under a nitrogen atmosphere at a heating rate of 10 °C/min using a Pyris 1 thermogravimetric analyzer (Perkin Elmer, USA). Scanning electron microscope/EDX were performed using SEM device (S360, Cambridge). TEM (Leo 906, Zeiss, Germany, 100 kV)
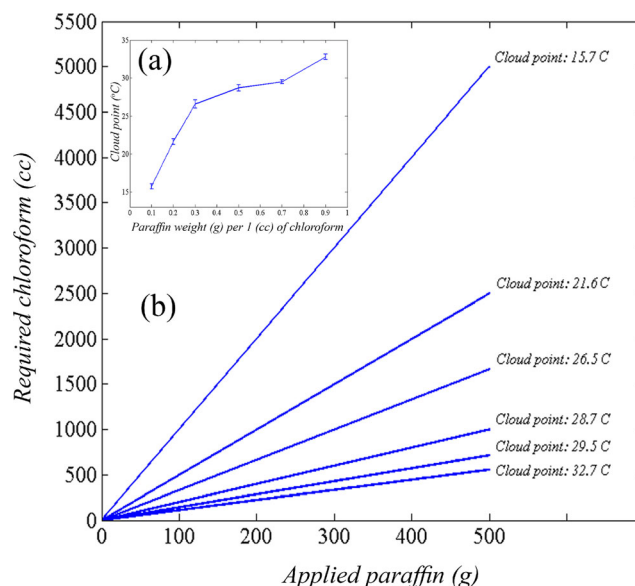

Fig. 2 **a** Cloud point temperature of chloroform/paraffin system as a function of paraffin content in 1 mL of chloroform. **b** The least required amount of chloroform per paraffin content at different process temperatures

was used in order to investigate the location of the produced JNPs in blend samples.

Result and discussion

Provided paraffin substrate covered with P1 or P2 nanoparticle were studied using FE-SEM images. As illustrated in Fig. 3, the test revealed the perfect coverage of paraffin substrates with P1 or P2 nanoparticles after the fixing process. This also confirmed the efficiency of heat-driven buoyancy flow as a fixing tool in the process. It should be noted that, in the case of P1 nanoparticles, the aggregates are formed due to the specific conditions of sample preparing stage for FE-SEM test. In order to prevent inflaming of paraffin, it was essential to decrease the device voltage which caused the formation of gold aggregates on the surface of paraffin substrates (covered with nanoparticles). Though, as it is shown in Fig. 3d, besides the mentioned limitation, some individual P2 nanoparticles can be distinguished on the surface of paraffin substrates.

Produced JNPs were studied by FTIR, TGA, and EDX tests in order to confirm attachment of modifier molecules on the surface of the nanoparticles after each stage. FTIR spectra of P1 and P2 JNPs and their corresponding bare nanoparticles are presented in Fig. 4. According to the results, the characteristic peaks in the ranges of 1100–1125 cm^{-1}, 810–820 cm^{-1}, and 470–480 cm^{-1} are attributed to Si-O-Si asymmetrical stretching vibrations [22], symmetrical stretching vibrations [23, 24], and bending vibrations [21–24],
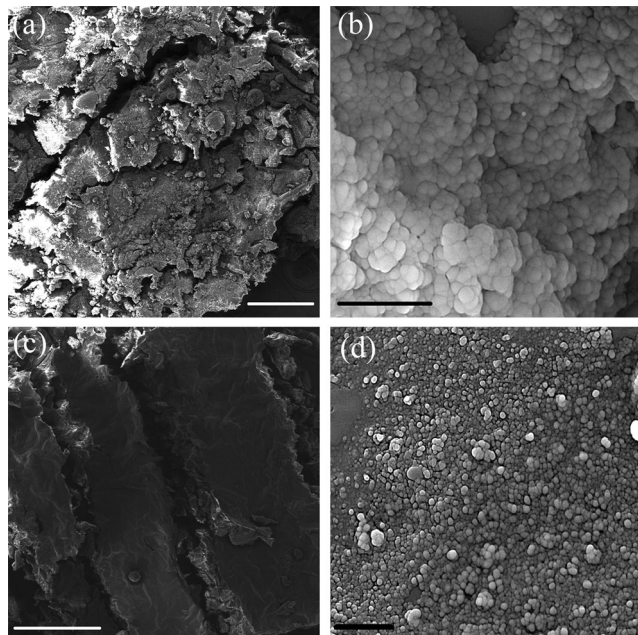

Fig. 3 The FE-SEM results of the provided paraffin substrates covered with **a**, **b** P1 nanoparticles and **c**, **d** P2 nanoparticles (*scale bar* = 500 μm in **a**, **c**; *scale bar* = 2 μm in **b**, **d**)
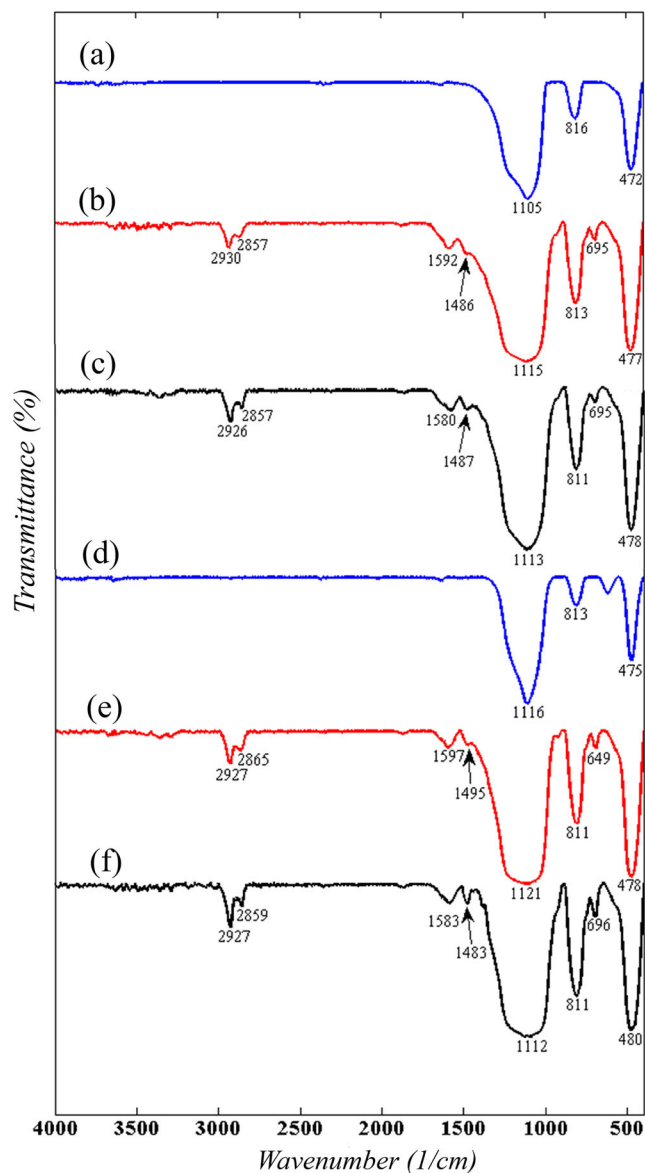

Fig. 4 FTIR spectroscopies of (*a*) bare P1 nanoparticles, (*b*) obtained P1 Janus nanoparticles from primary modification stage (P1p), (*c*) obtained P2 Janus nanoparticles from secondary modification stage (P1s), (*d*) bare P2 nanoparticles, (*e*) obtained P2 Janus nanoparticles from primary modification stage (P2p), and (*f*) obtained P2 Janus nanoparticles from secondary modification stage (P2s)

respectively. After modification with APTES (the primary modification stage, Fig. 4*b*, *e*), the small sharp peak at 695 cm^{-1} appears due to methyl rock vibrations. [23, 24] The peaks in the ranges of 1480–1500 cm^{-1} and 1580–1600 cm^{-1} correspond to C–H and NH$_2$ absorptions, respectively. [25] Also, peaks in the ranges of 2855–2875 cm^{-1} and 2925–2935 cm^{-1} are, respectively, ascribed to –CH$_2$ and C–H stretching vibrations [26]. It should be noted that the obtained P1 and P2 Janus nanoparticles from primary modification stage are referred as P1p and P2p, respectively. Also, the obtained Janus nanoparticles from the secondary modification

stage are mentioned as P1s and P2s. From the FTIR result of P1p and P2p (Fig. 4b, e), it could be concluded that APTES molecules were successfully attached to the exposed surface of P1 and P2 nanoparticles in primary modification stage. On the other hand, FTIR results of P1s and P2s (Fig. 4c, f) showed that almost all included peaks except that belonged to NH_2 in the range of 1580–1600 cm^{-1} were amplified due to the attachment of HDTMS molecules on the residual bare surface of the P1p and P2p nanoparticles. It should be also pointed out that in P1s and P2s, the peak in the range of 2925–2935 cm^{-1} was also attributed to CH_3 stretch vibration, besides C–H stretch bond, which was not expected in the P1p and P2p samples. [23].

TGA was also performed in order to calculate the grafting densities of APTES and HDTMS molecules on the surface of both nanoparticles (Fig. 5). The remaining weights of P1p and P1s were 83.31 and 80.31 wt.%, respectively. Also, the remaining weights of P2p and P2s were 82.91 and 81.67 wt.%, respectively. In all Janus samples, the first small amount of weight loss (~ 2 wt.%) was due to the evaporation of adsorbed water [27]. The second weight loss in both P1p and P2p samples was mainly due to the degradation of –NH_2 and –CH_2– groups (decomposition temperature range of APTES, 200–700 °C [28]). Accordingly, in the case of both P1s and P2s samples, the second weight loss was attributed to the degradations of –CH_3 group as well as –NH_2 and –CH_2– groups (decomposition temperature range of HDTMS, 300–

400 °C [29]). The weight loss of P1p sample was 12.84 wt.% while it was 15.04 wt.% for P1s. Moreover, the weight loss of P2p was 13.13 wt.% and the weight loss of P2s was 17.76 wt.%. As a result, the grafting density (molecule/nm^2) onto the surface of P1 and P2 JNPs was obtained 6.7 and 24.9, respectively. This shows an increment of the primary free silanol density on the surface of P1 and P2 nanoparticles (Table 1) as a result of rehydroxylation during the modification stages [30, 31] and/or crosslinking of the modifier molecules involving attached and unattached molecules. [32, 33].

As it is previously mentioned, three-phase contact angle (β) indicates the amphiphilic characteristics of the produced JNPs [14]. It defines the penetration depth of the spherical silica nanoparticles into the paraffin substrate (Scheme 3) and consequently indicates the modified surface in each modification stage and behavior of JNPs at interface regions (e.g., oil/water interface) [5, 34]. So far, many investigations have been performed to determine β, those are not useful in the case of small nanoparticles (< 50 nm) [5, 14, 34]. Herein, using TGA results, a new general method is proposed by which it is possible to calculate β for a wide size range of particles.

Assuming a Janus like particle, the number of degraded APTES molecules (N_{APTES}) can be calculated using Eq. (5):

$$N_{APTES} = \frac{(wl\%)_1 \times W_2 \times N_A}{M_{Ad}} \qquad (5)$$

where $(wl\%)_1$ is the weight loss percentage of the tested sample obtained from the primary modification stage, W_2 denotes the total weight of the tested sample obtained from the secondary modification stage, N_A is Avogadro's number, and M_{Ad} is the molecular weight of the degraded part of an individual APTES molecule. Similarly, the number of degraded HDTMS molecules (N_{HDTMS}) can be calculated using Eq. (6):

$$N_{HDTMS} = \frac{\{(wl\%)_2 - (wl\%)_1\} \times W_2 \times N_A}{M_{Hd}} \qquad (6)$$

where $(wl\%)_2$ is the weight loss percentage of the tested sample obtained from the second modification stage and M_{Hd}

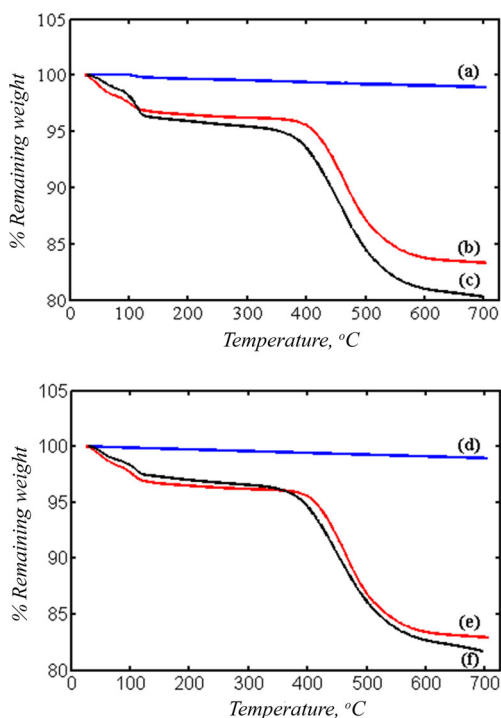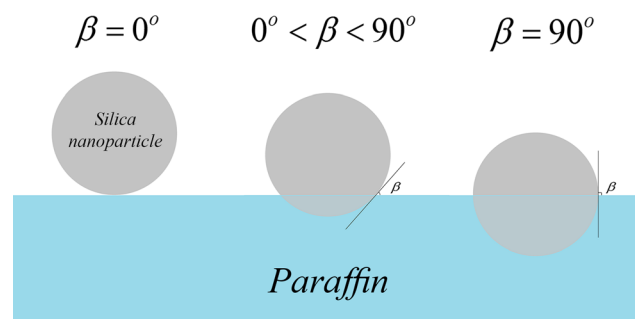Fig. 5 TGA results of (a) bare P1 nanoparticles, (b) P1p, (c) P1s, (d) bare P2 nanoparticles, (e) P2p, and (f) P2s

Scheme 3 Effects of β on the penetration depth of a spherical nanoparticle into paraffin

denotes the molecular weight of the degraded part of an individual HDTMS molecule. The number of silica nanoparticles (N_s) in the tested sample and their corresponding surface area (A_s) can be, respectively, indicated using Eqs. (7) and (8):

$$N_s = \frac{(100\% - (wl\%)_2) \times W_2}{\rho_{silica} \times V_s} \tag{7}$$

$$A_s = N_s \pi d^2 \tag{8}$$

where d and ρ_{silica} are the diameter and the density of nanoparticles. Thus, the number of attached molecules per nm^2 of nanoparticle surface area (φ_M) can be calculated using Eq. (9):

$$\varphi_M = \frac{N_{HDTMS} + N_{APTES}}{A_s} \tag{9}$$

Using Eq. (5)–(7), it is possible to calculate the number of attached APTES molecules (n_{mA}) and HDTMS molecules (n_{mH}) to the surface of an individual nanoparticle as follows:

$$n_{mA} = \frac{N_{APTES}}{N_S} \tag{10}$$

$$n_{mH} = \frac{N_{HDTMS}}{N_S} \tag{11}$$

Consequently, the surface area occupied by APTES (s_{mA}) and HDTMS molecules (s_{mH}) on an individual nanoparticle surface can be calculated using Eqs. (12) and (13), respectively:

$$s_{mA} = n_{mA} \times \varphi_M \tag{12}$$

$$s_{mH} = n_{mH} \times \varphi_M \tag{13}$$

It is considered that all available preferential silanol sites on the surface of silica nanoparticles were consumed during each modification process. Therefore, it is possible to take s_{mH} as the surface area of the unexposed part of an individual silica nanoparticle in primary modification stage. Accordingly, β can be calculated using Eq. (14):

$$\beta = \arccos\left\{1 - \frac{2s_{mH}}{\pi d^2}\right\} \tag{14}$$

Based on Eq. (14), β was calculated as 24.5° and 34.6° for P1 and P2 nanoparticles, respectively. The reason of less penetration depth of P1 nanoparticles compared to that of P2 nanoparticles was investigated using Young's equation for a spherical nanoparticle at oil/water interface (Eq. (15) [13]):

$$\cos\beta = \frac{|\gamma(PO) - \gamma(PW)|}{\gamma(OW)} \tag{15}$$

where $\gamma(PO)$, $\gamma(PW)$, and $\gamma(OW)$ denote the interfacial tension between particle/oil phase, particle/water phase, and oil phase/water phase, respectively. Considering almost the same

$\gamma(PO)$ and $\gamma(PW)$ for both P1 and P2 nanoparticle, it is $\gamma(OW)$ which drastically affects β. Surface tension of water increases with the size and the concentration of silica nanoparticles and this definitely increases $\gamma(OW)$ [34]. In order to prove the validity of the TGA results, we also indicated β from FE-SEM images based on our previous work (Supplementary information, sections S1) [35]. However, it is impossible to obtain β for P1 nanoparticles based on FE-SEM images, but the accordance of the results for P2 nanoparticle shows the validity of the proposed method (β (TGA) = 34.6° and β (FE-SEM) = 34.7 ± 0.5°).

Figure 6 illustrates the EDX map scan result of P1p and P1s which show the presence of modifier molecules on the surface of the applied nanoparticles. As it is clear, the number of carbon (C), silicon (Si), and oxygen (O) elements increased in the sample obtained from secondary modification stage which is attributed to the presence of HDTMS molecules. Moreover, it is obvious that the number of nitrogen (N) elements, indicated as white dots, is almost the same in both stages. The same results were obtained from the EDX map scan of P2p and P2s (Fig. 7).

Although the FTIR, TGA, and EDX tests gave good information about the attachment of modifier molecules on the surface of the nanoparticles, but another test was also used in order to prove their amphiphilic characteristics. In this test, JNPs provided from primary modification stage, were mixed with equal weight of silica nanoparticles which were uniformly modified with APTES. The uniform modification process was performed based on adding P1 or P2 nanoparticles to the mixture of methanol and APTES and stirring the system for 24 h [16, 36]. Then, JNPs and uniformly modified nanoparticles were dispersed in a mixture of water and dichloromethane and centrifuged. Figure 8a, c shows that JNPs are exactly placed at the water/dichloromethane interface as amphiphilic particles [10] and uniformly modified silica nanoparticles are cumulated in chloroform phase which is attributed to their tendency to the organic solvent. As it is illustrated in Fig. 8b, d, JNPs provided from primary modification stage also tend to be placed at the interface even without centrifuging. Therefore, it can be concluded that there were no aggregation of nanoparticles on the surface of paraffin substrate at fixing stage since the aggregating causes the formation of impurities (uniformly modified nanoparticles or unmodified ones) after primary modification stage. Accordingly, if such impurities exist among JNPs, there should be a dispersion of nanoparticles in dichloromethane/water system as JNPs tend to be placed at the interface, unmodified nanoparticles disperse in water, and uniformly modified nanoparticles disperse in dichloromethane.

In another attempt, we investigated the behavior of the provided P2 JNPs from secondary modification stage and the homogeneously modified P2 nanoparticles with both APTES and HDTMS in dichloromethane/water system.

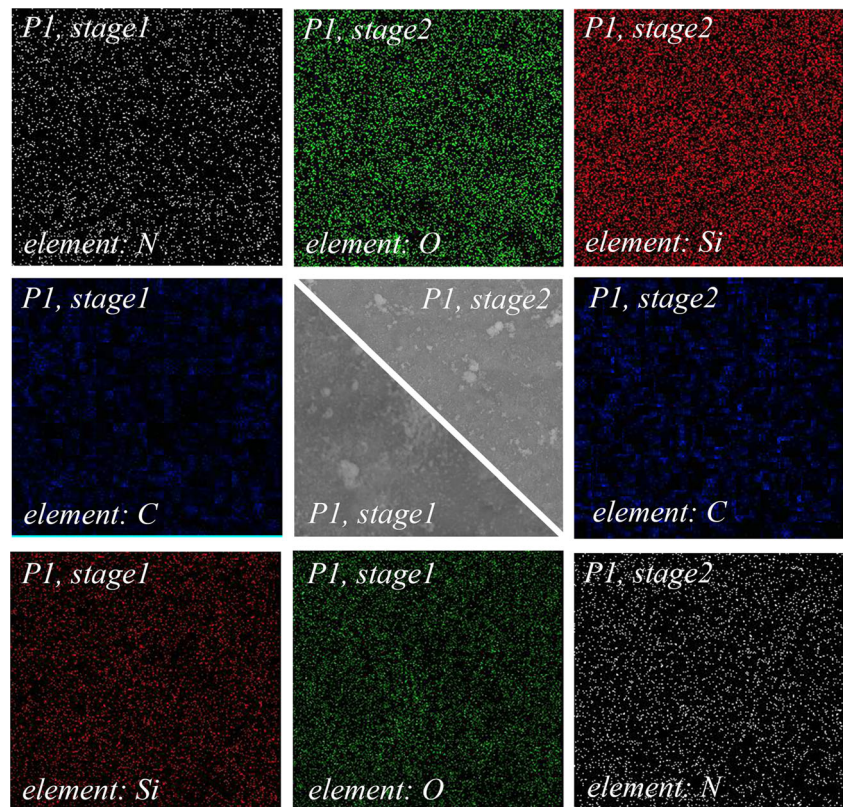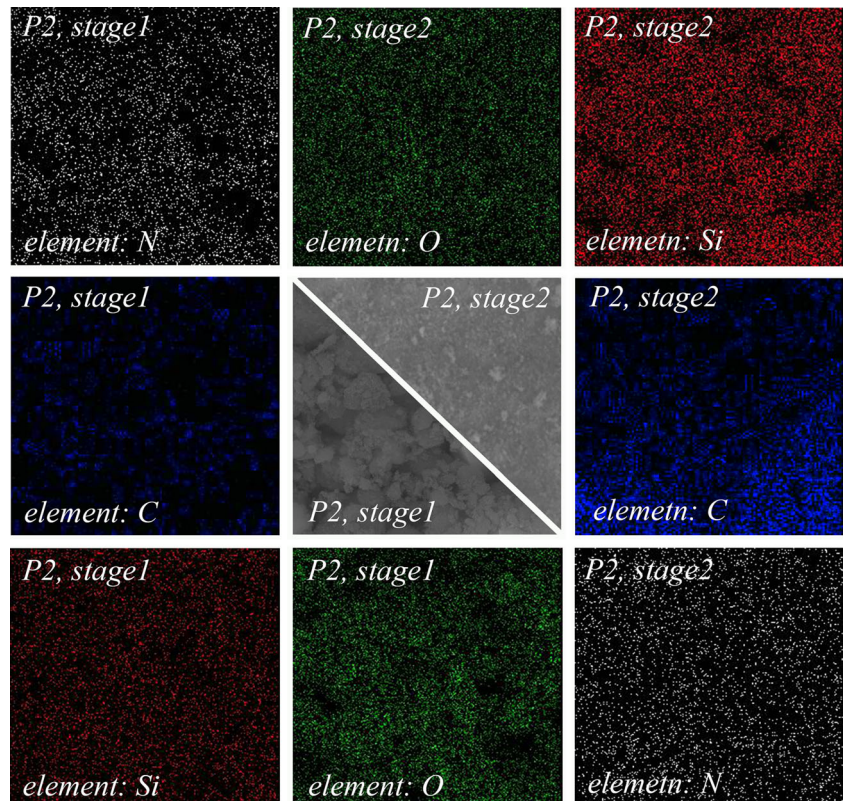**Fig. 6** EDX map scan results of the P1p and P1s samples

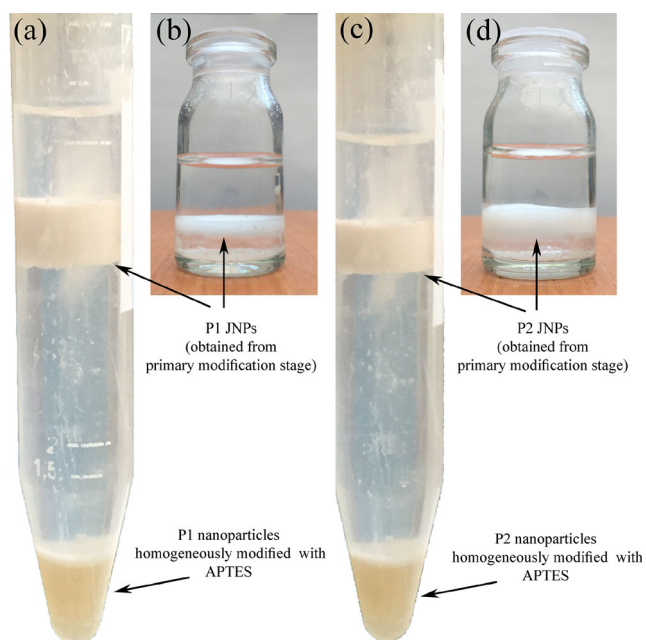**Fig. 7** EDX map scan results of the P2p and P2s samples

Fig. 8 The location of **a** P1 Janus (obtained from primary modification stage) and homogeneously modified nanoparticles, **b** P1 JNPs (obtained from primary modification stage), **c** P2 Janus (obtained from primary modification stage) and homogeneously modified nanoparticles, and **d** P2 JNPs (obtained from primary modification stage) in dichloromethane/water systems. *Upper phase*: water, *lower phase*: dichloromethane

Fig. 9 The location of **a** P2 JNPs (obtained from secondary modification stage) and **b** P2 nanoparticles homogeneously modified with APTES and HDTMS in dichloromethane/water system. *Upper phase*: water, *lower phase*: dichloromethane

The homogenous modification of P2 nanoparticles was performed based on the following method.

At first, P2 nanoparticles were uniformly modified with APTES using the protocol described before. Then, after washing the nanoparticles with methanol, modification process was continued in methanol media containing HDTMS for 24 h.

As it is illustrated in Fig. 9a, P2 JNPs dispersed in dichloromethane phase while the homogeneously modified nanoparticles dispersed through the system. It should be noted that, the behavior of P2 JNPs was completely expected since their major surface portion was modified with APTES and the attachment of HDTMS molecules to their bare side (after secondary modification stage) increased their hydrophobicity. This made the provided JNPs from the primary modification stage to migrate from the interface into the dichloromethane phase (after the secondary modification stage). Therefore, the bare side plays an important role in forming amphiphilic properties of JNPs (provided from primary modification stage) and helps them to be placed at dichloromethane/water interface. On the other hand, the homogeneously modification of nanoparticles induced random surface characteristics to the nanoparticles and caused them to disperse in different phases (including interface).

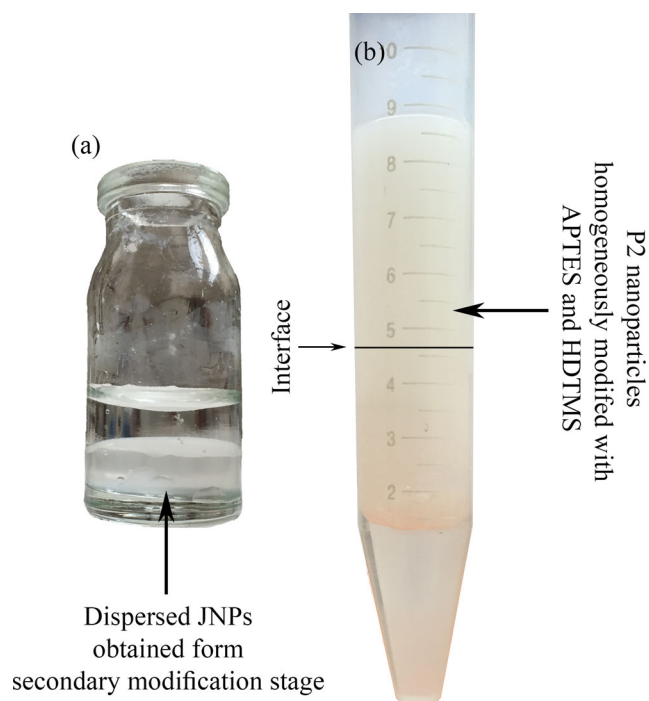In order to further investigating the behavior of the final produced JNPs, some PS/PMMA blends containing P2 JNPs, P2 nanoparticles homogeneously modified with APTES, and P2 nanoparticles homogeneously modified with HDTMS were prepared based on the following method:

All PS/PMMA (85/15 vol%) blend samples were prepared via solution mixing. For preparing samples containing JNPs and nanoparticles homogeneously modified with APTES, at the first step, PMMA was dissolved in dichloromethane and after complete dissolution, nanoparticles (3 wt%) were added under agitation. Accordingly, nanoparticles homogeneously modified with HDTMS were added to the solution of PS in dichloromethane. After 45 min, the second polymer phase was added and after complete dissolution the mixing continued for 45 min. Thereafter, the samples were casted in a glass petri dish for 7 days in room temperature and then they were held under vacuum at 60 °C for 48 h in order to extract the remaining solvent.

As it is illustrated in Fig. 10, P2 JNPs were placed at the interface while P2 nanoparticles homogeneously modified with APTES, and HEXA were dispersed in PMMA and PS phases, respectively. Based on the results of the performed test in dichloromethane/water system, the produced JNPs acted as expected in PS/PMMA samples.

Based on the similarity of P1 and P2 JNPs test results, it was proved that the proposed process acts perfectly in producing JNPs of different sizes.

Fig. 10 **a**, **b** P2 JNPs at the interface of PS and PMMA phases, **c** P2 nanoparticles homogeneously modified with APTES placed in PMMA phase, and **d** P2 nanoparticles homogeneously modified with HDTMS placed in PS phase
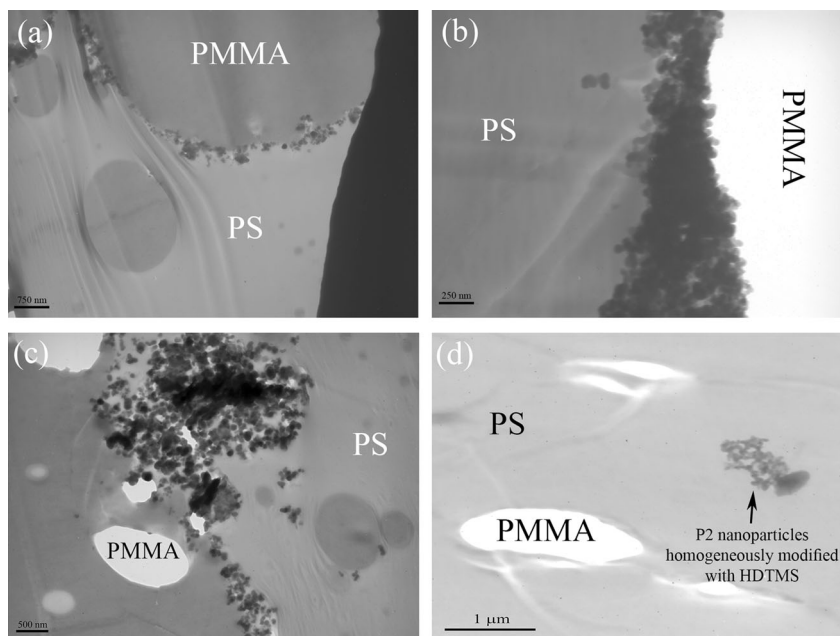
Conclusion

A new and unique desymmetrization method was used in order to produce Janus nanoparticles applying oil (melted wax)/water dual-phase system. The process consisted of four stages: fixing, primary modification, releasing, and secondary modification. Unlike other similar works, there was no limited or partial coalescence in the system which prevented the presence of impurities (unmodified or uniformly modified nanoparticles) in the final production. Dispersed hydrophilic nanoparticles in the water phase were forced to be placed at oil/water interface using heat-derive buoyancy flow formed by the applied heat at the bottom of the container. Saturation theory (ST) was used in order to indicate the minimum content of nanoparticles considering the optimum effects of upward induced water stream. The content of all system constituents was precisely indicated to prevent material waste as well as controlling the effective system parameters, e.g., complete elimination of paraffin wax in releasing stage. This was introduces as one of the advantageous of the proposed process which makes it more efficient compared to the other related works. After each modification stage, the produced Janus nanoparticles were investigated using FTIR, TGA, and EDX in order to confirm the attachment of modifier molecules on the surface of the nanoparticles. Furthermore, TGA results were used in order to indicate three-phase contact angle (β) which revealed the asymmetrical nature of the produced Janus nanoparticles. β was also indicated using FE-SEM images of the fixed nanoparticles on the surface of solid paraffin base in order to approve TGA results. Accordingly, it was proved that the

available surface area of the nanoparticles in each corresponding modification stage was completely modified via a particular modifying agent. The amphiphilic property of the produced JNPs (provided form primary modification stage) was also investigated via dispersing them in a dual-phase dichloromethane/water media. Comparing produced JNPs with uniformly modified silica nanoparticles (with APTES) revealed that JNPs tended to be placed at the interface of the organic/inorganic system while the uniformly modified silica nanoparticles cumulated in dichloromethane phase. Accordingly, it was shown that homogeneously modification of nanoparticles induces random characteristics to the surface of nanoparticles while it is possible to engineer it using desymmetrization process. This was approved by applying the produced JNPs, homogeneously modified nanoparticles with APTES and homogeneously modified nanoparticles with HDTMS in PS/PMMA blend. The results showed the aggregation of JNPs at the interface while homogeneously modified nanoparticles with APTES and HDTMS were dispersed in PMMA and PS phases, respectively. Moreover, it was demonstrated that the proposed desymmetrization process is very simple to use and has good economical and qualitative efficiencies compared to common desymmetrization process.

References

1. Rotello V (2012) Nanoparticles: building blocks for nanotechnology. Springer, US
2. Kango S, Kalia S, Celli A, Njuguna J, Habibi Y, Kumar R (2013) Surface modification of inorganic nanoparticles for development of organic–inorganic nanocomposites—a review. Prog Polym Sci 38(8):1232–1261. doi:10.1016/j.progpolymsci.2013.02.003
3. Mahdavi M, Ahmad M, Haron M, Namvar F, Nadi B, Rahman M, Amin J (2013) Synthesis, surface modification and characterisation of biocompatible magnetic iron oxide nanoparticles for biomedical applications. Molecules 18(7):7533. doi:10.3390/molecules18077533
4. Caruso F (2001) Nanoengineering of particle surfaces. Adv Mater 13(1):11–22. doi:10.1002/1521-4095(200101)13:1<11::AID-ADMA11>3.0.CO;2-N
5. Hong L, Cacciuto A, Luijten E, Granick S (2006) Clusters of charged Janus spheres. Nano Lett 6(11):2510–2514. doi:10.1021/nl061857i
6. Iacovella CR, Horsch MA, Zhang Z, Glotzer SC (2005) Phase diagrams of self-assembled mono-tethered nanospheres from molecular simulation and comparison to surfactants. Langmuir 21(21):9488–9494. doi:10.1021/la051035l
7. Lv W, Lee KJ, Li J, Park T-H, Hwang S, Hart AJ, Zhang F, Lahann J (2012) Anisotropic Janus catalysts for spatially controlled chemical reactions. Small 8(20):3116–3122. doi:10.1002/smll.201200192
8. Dendukuri D, Doyle PS (2009) The synthesis and assembly of polymeric microparticles using microfluidics. Adv Mater 21(41):4071–4086. doi:10.1002/adma.200803386
9. Shah RK, Kim J-W, Weitz DA (2009) Janus supraparticles by induced phase separation of nanoparticles in droplets. Adv Mater 21(19):1949–1953. doi:10.1002/adma.200803115
10. Perro A, Meunier F, Schmitt V, Ravaine S (2009) Production of large quantities of "Janus" nanoparticles using wax-in-water emulsions. Colloids Surf 332(1):57–62. doi:10.1016/j.colsurfa.2008.08.027
11. Pickering SU (1907) CXCVI.—emulsions. J Chem Soc Trans 91(0):2001–2021. doi:10.1039/CT9079102001
12. Walther A, Müller AHE (2013) Janus particles: synthesis, self-assembly, physical properties, and applications. Chem Rev 113(7):5194–5261. doi:10.1021/cr300089t
13. Pieranski P (1980) Two-dimensional interfacial colloidal crystals. Phys Rev Lett 45(7):569–572. doi:10.1103/PhysRevLett.45.569
14. Jiang S, Granick S (2008) Controlling the geometry (Janus balance) of amphiphilic colloidal particles. Langmuir 24(6):2438–2445. doi:10.1021/la703274a
15. Giermanska-Kahn J, Laine V, Arditty S, Schmitt V, Leal-Calderon F (2005) Particle-stabilized emulsions comprised of solid droplets. Langmuir 21(10):4316–4323. doi:10.1021/la0501177
16. Hong L, Jiang S, Granick S (2006) Simple method to produce Janus colloidal particles in large quantity. Langmuir 22(23):9495–9499. doi:10.1021/la062716z
17. Hemmer E, Quintanilla M, Légaré F, Vetrone F (2015) Temperature-induced energy transfer in dye-conjugated Upconverting nanoparticles: a new candidate for Nanothermometry. Chem Mater 27(1):235–244. doi:10.1021/cm503799f
18. Nasrin R, Alim MA, Chamkha AJ (2012) Buoyancy-driven heat transfer of water–Al2O3 nanofluid in a closed chamber: effects of solid volume fraction, Prandtl number and aspect ratio. Int J Heat Mass Transf 55(25–26):7355–7365. doi:10.1016/j.ijheatmasstransfer.2012.08.011
19. Adam NK (1952) The physics and chemistry of surfaces. Oxford University Press, Oxford
20. Maghsoud Z, Navid Famili MH, Madaeni SS (2010) Phase diagram calculations of water/tetrahydrofurane/poly (vinyl chloride) ternary system based on a compressible regular solution model. Iran Polym J 19(8):581–588
21. Barzin J, Sadatnia B (2007) Theoretical phase diagram calculation and membrane morphology evaluation for water/solvent/polyethersulfone systems. Polymer 48(6):1620–1631. doi:10.1016/j.polymer.2007.01.049
22. Amirshaqaqi N, Salami-Kalajahi M, Mahdavian M (2014) Investigation of corrosion behavior of aluminum flakes coated by polymeric nanolayer: effect of polymer type. Corros Sci 87:392–396. doi:10.1016/j.corsci.2014.06.045
23. Lambert JB (1987) Introduction to organic spectroscopy. Macmillan, London
24. Xu L, Wang L, Shen Y, Ding Y, Cai Z (2015) Preparation of hexadecyltrimethoxysilane-modified silica nanocomposite hydrosol and superhydrophobic cotton coating. Fibers and Polymers 16(5):1082–1091. doi:10.1007/s12221-015-1082-x
25. Samadaei F, Salami-Kalajahi M, Roghani-Mamaqani H, Banaei M (2015) A structural study on ethylenediamine- and poly (amidoamine)-functionalized graphene oxide: simultaneous reduction, functionalization, and formation of 3D structure. RSC Adv 5(88):71835–71843. doi:10.1039/C5RA12086A
26. Amirshaqaqi N, Salami-Kalajahi M, Mahdavian M (2014) Corrosion behavior of aluminum/silica/polystyrene nanostructured hybrid flakes. Iran Polym J 23(9):699–706. doi:10.1007/s13726-014-0264-5
27. Panahian P, Salami-Kalajahi M, Salami Hosseini M (2014) Synthesis of dual Thermosensitive and pH-sensitive hollow Nanospheres based on poly (acrylic acid-b-2-hydroxyethyl methacrylate) via an atom transfer reversible addition–fragmentation radical process. Ind Eng Chem Res 53(19):8079–8086. doi:10.1021/ie500892b
28. Maity D, Chandrasekharan P, Feng S-S, Jun D (2010) Synthesis and studies of APTES functionalized magnetite nanoparticles. In: Nanoscience and Nanotechnology (ICONN), 2010 International Conference on, . IEEE, pp 94–97
29. Paopattra T, Sarintorn L, Kawee S (2012) Preparation of organosilane treated microcrystalline (SiMCC) and SiMCC/polypropylene composites. Journal of Metals, Materials and Minerals 22:13–19
30. Zhuravlev LT (2000) The surface chemistry of amorphous silica. Zhuravlev model. Colloids Surf 173(1–3):1–38. doi:10.1016/S0927-7757(00)00556-2
31. Shioji S, Kawaguchi M, Hayashi Y, Tokami K, Yamamoto H (2001) Rehydroxylation of dehydrated silica surfaces by water vapor adsorption. Adv Powder Technol 12(3):331–342. doi:10.1163/156855201750537884
32. Acres RG, Ellis AV, Alvino J, Lenahan CE, Khodakov DA, Metha GF, Andersson GG (2012) Molecular structure of 3-Aminopropyltriethoxysilane layers formed on silanol-terminated silicon surfaces. J Phys Chem C 116(10):6289–6297. doi:10.1021/jp212056s
33. Liu Y, Li Y, Li X-M, He T (2013) Kinetics of (3-aminopropyl)triethoxylsilane (APTES) silanization of superparamagnetic iron oxide nanoparticles. Langmuir 29(49):15275–15282. doi:10.1021/la403269u
34. Bhuiyan MHU, Saidur R, Amalina MA, Mostafizur RM, Islam A (2015) Effect of nanoparticles concentration and their sizes on surface tension of nanofluids. Procedia Engineering 105:431–437. doi:10.1016/j.proeng.2015.05.030
35. Sharifzadeh E, Salami-Kalajahi M, Hosseini MS, Aghjeh MKR (2016) A temperature-controlled method to produce Janus nanoparticles using high internal interface systems: experimental and theoretical approaches. Colloids Surf 506:56–62. doi:10.1016/j.colsurfa.2016.06.006
36. Vansant EF, Van Der Voort P, Vrancken KC (1995) Characterization and chemical modification of the silica surface. Elsevier Science, New York